



Recent Star Formation in $0.5 < z < 1.5$ Quiescent Galaxies

Michael J. Rutkowski¹, Bonnabelle Zabelle², Tyler Hagen³, Anahita Alavi⁴, Seth Cohen⁵, Christopher Conselice⁶, Norman Grogin⁷, Yicheng Guo⁸, Matthew Hayes⁹, Sugata Kaviraj¹⁰, Anton Koekemoer⁷, Ray A. Lucas⁷, Kameswara Bharadwaj Mantha², Alec Martin⁸, Vihang Mehta⁴, Bahram Mobasher¹¹, Nimish Hathi⁷, Zhiyuan Ji¹², Kalina V. Nedkova^{7,13}, Robert O’Connell¹⁴, Marc Rafelski⁷, Claudia Scarlata², Harry I. Teplitz⁴, Xin Wang^{15,16,17}, Rogier Windhorst⁵, L. Y. Aaron Yung⁷ and The UVCANDELS Team

¹ Minnesota State University-Mankato, Department of Physics & Astronomy, Trafton Science Center North 141, Mankato, MN 56001, USA; michael.rutkowski@mnsu.edu

² Minnesota Institute for Astrophysics, University of Minnesota, 116 Church St. SE, Minneapolis, MN 55455, USA

³ University of Utah, Department of Physics & Astronomy, 115 S. 1400 E., Salt Lake City, UT 84112-0830, USA

⁴ IPAC, California Institute of Technology, 1200 E. California Blvd., Pasadena, CA 91125, USA

⁵ School of Earth and Space Exploration, Arizona State University, Tempe, AZ 85287, USA

⁶ School of Physics and Astronomy, The University of Nottingham, University Park, Nottingham NG7 2RD, UK

⁷ Space Telescope Science Institute, 3700 San Martin Drive, Baltimore, MD 21218, USA

⁸ Department of Physics and Astronomy, University of Missouri, Columbia, MO 65211, USA

⁹ Stockholm University, Department of Astronomy and Oskar Klein Centre for Cosmoparticle Physics, SE-10691, Stockholm, Sweden

¹⁰ Centre for Astrophysics Research, University of Hertfordshire, Hatfield, AL10 9AB, UK

¹¹ Department of Physics and Astronomy, University of California, Riverside, Riverside, CA 92521, USA

¹² University of Massachusetts Amherst, 710 N. Pleasant Street, Amherst, MA 01003-9305, USA

¹³ Department of Physics and Astronomy, Johns Hopkins University, Baltimore, MD 21218, USA

¹⁴ Department of Astronomy, University of Virginia, Charlottesville, VA 22904, USA

¹⁵ School of Astronomy and Space Science, University of Chinese Academy of Sciences (UCAS), Beijing 100049, People’s Republic of China

¹⁶ National Astronomical Observatories, Chinese Academy of Sciences, Beijing 100101, People’s Republic of China

¹⁷ Institute for Frontiers in Astronomy and Astrophysics, Beijing Normal University, Beijing 102206, People’s Republic of China

Received 2024 December 11; revised 2025 February 9; accepted 2025 March 7; published 2025 April 14

Abstract

Observations of massive, quiescent galaxies reveal a relatively uniform evolution: following prolific star formation in the early Universe, these galaxies quench and transition to their characteristic quiescent state in the local Universe. The debate on the relative role and frequency of the process(es) driving this evolution is robust. In this Letter, we identify $0.5 \lesssim z \lesssim 1.5$ massive, quiescent galaxies in the Hubble Space Telescope/UVCANDELS extragalactic deep fields using traditional color selection methods and model their spectral energy distributions, incorporating novel UV images. This analysis reveals $\sim 15\%$ of massive, quiescent galaxies have experienced minor, recent star formation ($< 10\%$ of total stellar mass within the past ~ 1 Gyr). We find only a marginal, positive correlation between the probability for recent star formation and a measure of the richness of the local environment from a statistical analysis. Assuming the recent star formation present in these quiescent galaxies is physically linked to the local environment, these results suggest only a minor role for dynamic external processes (galaxy mergers and interactions) in the formation and evolution of these galaxies at this redshift.

Unified Astronomy Thesaurus concepts: Galaxy evolution (594); Ultraviolet astronomy (1736)

1. Introduction

The development of a robust model of the transformation of high-redshift star-forming galaxies into quiescent galaxies observed in the local Universe is a primary goal in the study of galaxy evolution. Massive quiescent galaxies, specifically, are an appealing class for study in the development of such models. Historically, diverse lines of observational evidence—e.g., optical colors, inferred star formation histories (SFHs), and α -element enhancement (e.g., R. G. Bower et al. 1992, A. Heavens et al. 2004, and J. Johansson et al. 2012, respectively)—have been interpreted as evidence for a common evolutionary history, whereby quiescent galaxies descended from galaxies in the early Universe that rapidly assembled, ceased star formation (quench), and evolved quiescently until the present day.

Extensive surveys have measured the declining quiescent fraction (with a commensurate increase in stellar mass density arising from the quenching of galaxies) with increasing redshift, since $z \lesssim 4$ (O. Ilbert et al. 2013; A. Muzzin et al. 2013). More recently, massive quiescent galaxies have been identified in the first ~ 2 Gyr (at $z \sim 4$; K. Glazebrook et al. 2017; F. Valentino et al. 2020) that have recently quenched intense star formation. JWST is dramatically advancing the state of the art, detecting similar mass, quenched galaxies at higher redshifts ($z > 4$; A. C. Carnall et al. 2023a, 2023b; A. de Graaff et al. 2025) while also revealing possible progenitors ($z \gg 5$, low-mass galaxies) effectively “caught in the act,” transitioning to quiescence through (mini) quenching events (V. Strait et al. 2023; T. J. Looser et al. 2024) with the clear spectroscopic signatures of the characteristic rapid star formation, quenching, and declining star formation rate (SFR) thereafter. In cosmological simulations, a combination of “in situ” (stellar and active galactic nucleus (AGN) feedback; Y. Dubois et al. 2013; K. El-Badry et al. 2016) and “external” (i.e., environmental; S. Kaviraj et al. 2015) processes are

typically invoked to broadly reproduce the evolution of this class of galaxies toward the quiescent state.

But, refining this general evolutionary scenario is necessary to accommodate a variety of key observational caveats. First, a substantial fraction (exceeding $\sim 20\%$ at $z \lesssim 2$) of quenched or quiescent galaxies exhibit recent star formation (RSF; S. Kaviraj et al. 2007, 2008; M. J. Rutkowski et al. 2014; K. Kim et al. 2018; E. D. Paspaliaris et al. 2023), and may do so repeatedly, via mini-quenching events that only temporarily halt star formation (T. Dome et al. 2024; V. Gelli et al. 2025). Depending on the epoch in which these galaxies are observed during this process, the inferred SFH for such galaxies may not exhibit the form characteristic of these galaxies—a uniform, single, exponentially declining SFH with $\text{SFR} \propto \exp(-t/\tau)$ —that is typically used for preselection (on specific SFR, e.g., S. Salim et al. 2018).

Second, the relative predominance of the varied physical processes responsible for the transformation of quiescent galaxies over time is uncertain. Considering only mergers, their impact is diverse and varied. Recognizing that recent observations indicate a likely mass-dependent effect (S. E. Cutler 2024), RSF in quiescent galaxies is likely a result of mergers or accretion (S. Kaviraj et al. 2013; C. Cleland & S. L. McGee 2021). Further, the episodic accretion of low-mass satellites could (in theory, see T. Naab et al. 2009) motivate their observed size–mass growth (P. Cassata et al. 2011; R. E. J. Ryan et al. 2012). In contrast, major mergers are implicated in the rapid quenching of star formation (K. Bekki et al. 2005; M. E. Verrico et al. 2023) in galaxies that subsequently manifest as quiescent, poststarburst (PSB) galaxies (which are observed preferentially in richer environments; B. M. Poggianti et al. 2009).

Large surveys of RSF in quiescent galaxies can provide insight into these complex, stochastic mechanisms and the frequency and duration of the quenching process (V. Wild et al. 2016; F. Belfiore et al. 2018; M. Clausen et al. 2024). In particular, when rest-frame UV-optical–near-IR photometry is available for quiescent galaxies, it is possible to uniquely characterize the age, mass fraction, and SFH of RSF.

Only Hubble Space Telescope (HST) WFC3/UVIS can provide high ($\ll 1''$) resolution¹⁸ rest-frame UV imaging of $0.5 < z < 1.5$ galaxies, but prior to HST Cycle 26, only $\sim 100 \text{ arcmin}^2$ in total had broadband rest-frame far-UV imaging and the longer wavelength imaging necessary for characterizing the predominant, old stellar population.

In this Letter, we directly search for RSF in quiescent galaxies in new UV extragalactic survey data. Throughout this Letter, we assume a Planck concordance model (Planck Collaboration et al. 2016); we report magnitudes as AB magnitudes (J. B. Oke & J. E. Gunn 1983).

2. UVCANDELS Imaging and Photometry

UVCANDELS obtained WFC3/UVIS F275W and Advanced Camera for Surveys (ACS) F435W images over $\sim 450 \text{ arcmin}^2$ in four extragalactic deep fields (COSMOS, Extended Groth Strip (EGS), GOODS-North, and GOODS-South) to a depth of $AB = 27$ (3σ point source). To date, this UV imaging has already supported diverse analyses in Lyman continuum escape (B. M. Smith et al. 2024), resolved star formation (V. Mehta et al. 2023; K. V. Nedkova et al. 2024), and quiescent galaxies (B. Zabelle et al. 2023). Combined with the rich

multiwavelength imaging and spectroscopy available for these fields, UVCANDELS effectively *quadruples* the area in which RSF can be directly probed in $z \sim 1$ massive, quiescent galaxies, as F275W and F435W are sensitive to $1600 \lesssim \lambda[\text{\AA}] \lesssim 2000$ and $2500 \lesssim \lambda[\text{\AA}] \lesssim 3200$ ($960 \lesssim \lambda[\text{\AA}] \lesssim 1200$ and $1500 \lesssim \lambda[\text{\AA}] \lesssim 2000$) at $z \sim 0.5$ ($z \sim 1.5$).

We refer the reader to X. Wang et al. (2025) and V. Mehta et al. (2024) for full details, but reiterate key components of the data processing here. Namely, custom routines produced by M. Rafelski et al. (2015) and L. J. Prichard et al. (2022) were adapted for use in the calibration of these UVCANDELS data, including corrections for charge transfer efficiency according to J. Anderson et al. (2021). In addition, the images were individually corrected with custom hot pixel masks including readout cosmic rays, scattered light (see J. Biretta et al. 2003), and any 2D background gradient across the entire CCD chips. The data were registered and stacked within a pipeline adapted from A. Alavi et al. (2014) using AstroDrizzle to combine the calibrated, flat fielded WFC3/UVIS and ACS/WFC images. Images were produced with 30 mas pixels and aligned to the CANDELS astrometric reference grid at a precision of 0.15 pixel, using unsaturated stars and compact sources. These UVCANDELS imaging data reach a depth of $AB = 27$ (28) for compact galaxies in the WFC3/UVIS F275W (ACS/F435W). The final mosaicked data products are now available on MAST (H. Teplitz et al. 2022).

3. Quiescent Galaxies at $0.5 \leq z \leq 1.5$

This survey used extensive, deep optical–near-IR imaging and spectroscopy ($m \lesssim 26$ AB) from MAST,¹⁹ including HST/ACS CANDELS broadband imaging (N. A. Grogin et al. 2011; A. M. Koekemoer et al. 2011) and HST/IR G141 grism spectroscopy with ancillary catalogs (I. G. Momcheva et al. 2016) that combined these grism data with extensive ground-based observations.

Sample selection was first made on well-determined massive ($M_* \geq 10^{10} M_\odot$) galaxies at intermediate redshift ($0.5 \leq z \leq 1.5$), using 3DHST data products accessed via MAST. Next, using the value-added catalogs (I. G. Momcheva et al. 2016), we applied a rest-frame UVJ color–color criterion, and removed galaxies matched to X-ray detections within $0''.5$ (83 total; D. Kocevski 2025, private communication), which we assume to indicate AGN. We identified a total of 1067 quiescent galaxies; falsecolor images of a subsample of these galaxies is illustrated in Figure 1. We matched these galaxies on position, identifying matches within $0''.1$ between the coaligned 3DHST and UVCANDELS catalogs. We define the statistics for galaxies in Table 1. In Figure 2, we present general physical characteristics of the full sample.

4. Characterization of $0.5 \leq z \leq 1.5$ Quiescent Galaxies

4.1. Quiescent Galaxy Morphologies

To assess quiescent galaxy morphology, we used GALFIT (Y.-j. Peng et al. 2010) to fit Sérsic models to CANDELS WFC3-IR/F125W 30 mas imaging of the UVJ-selected sample. At $0.5 < z < 1.5$, F125W is sensitive exclusively to the spectral energy distribution (SED) *redward* of the 4000 \AA break and thus probes stellar emission from the old extant population. In

¹⁸ AstroSat UVIT/N242W can image at comparable wavelengths to HST UVIS F275W but at $\sim 5\times$ lower spatial resolution.

¹⁹ <https://archive.stsci.edu/prepds/3d-hst>

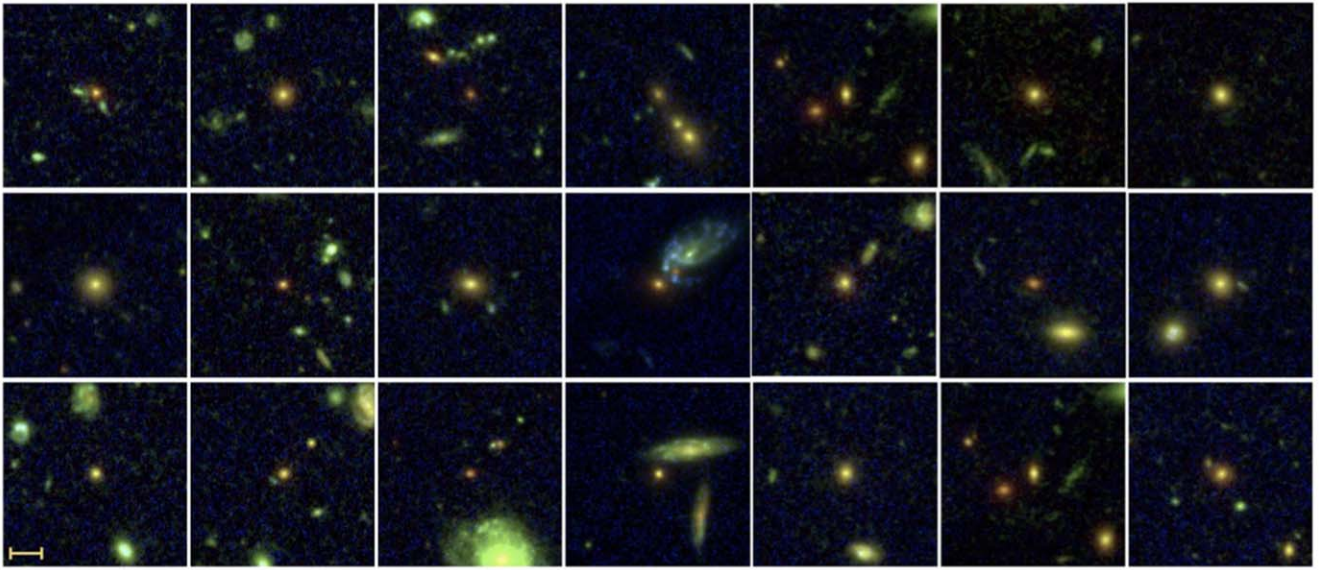


Figure 1. Representative three-color images of UVJ-selected, quiescent galaxies in the UVCANDELS fields considered in this survey. We combine UVCANDELS and archival imaging in WFC3/UVIS F275W, ACS/WFC F606W, and WFC3/IR F125W (blue, green, red, respectively). The quiescent galaxy is centered in each image; a scale bar of length $\sim 2''$ is provided (bottom left pane).

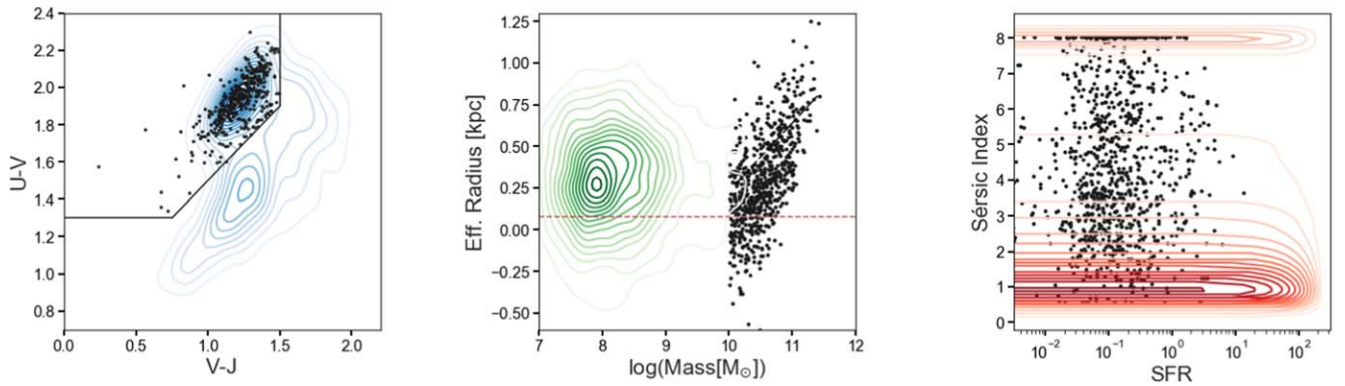


Figure 2. Relevant archival parameters derived for the UVCANDELS sample of quiescent galaxies; throughout, filled circles indicate significantly ($>3\sigma$) F275W-detected quiescent galaxies. Left panel: UVJ color–color used for differentiating $0.5 < z < 1.5$ quiescent galaxies (upper left) from SFGs; rest-frame UVJ colors from I. G. Momcheva et al. (2016). Center panel: physical size (kpc)–stellar mass distribution (M_{\odot}) with the same CANDELS field galaxies (green contours), with the HST WFC3-IR/F160W PSF FWHM in physical units ($z \simeq 1$). Right panel: Sérsic profile index–star formation rate ($M_{\odot} \text{ yr}^{-1}$) distribution with the same for CANDELS field galaxies (red contours). In the center and right panels, physical size parameters are from A. van der Wel et al. (2012) and stellar parameters are from I. G. Momcheva et al. (2016).

Table 1
Quiescent Galaxy Selection and Derived Samples

Selection Criteria	EGS	COSMOS	GOODS-N	GOODS-S	Total
UVJ-selected quiescent galaxies	312	413	259	83	1067
WFC3/F275W detection ($>3\sigma$)	37	38	48	18	141
WFC3/G141 emission line ($H\alpha > 5\sigma$)	8	7	6	3	24

Note. Tabulated galaxies were selected with $M_{*} > 10^{10} M_{\odot}$ at redshift $0.5 \leq z \leq 1.5$ in the footprint common to UVCANDELS and 3DHST. “Quiescent” galaxies selected on UVJ colors following R. J. Williams et al. (2009) are provided in the first row here; in the second row, UV-detected, X-ray nondetections. In the third row, we report the number of galaxies with significant $H\alpha$ emission (5σ), reported by I. G. Momcheva et al. (2016). For further discussion of these samples, see Section 3.

this analysis, we enforced two constraints when implementing GALFIT: (1) effective radius, r_e : $0.5 \text{ pixels} \lesssim r_e \lesssim 100 \text{ pixels}$ (or equivalently, $r_e \lesssim 3''/5$); and (2) Sérsic index, n : $0.5 \lesssim n \lesssim 8$. Here, the effective radius corresponds to the “half-light” radius,

or the inner radius containing half of the total flux in the best-fitting Sérsic model fit.

The majority were well fit ($\chi^2_{\nu} \lesssim 5$), and we measured an average Sérsic index of $n \simeq 4$ (to surface brightness

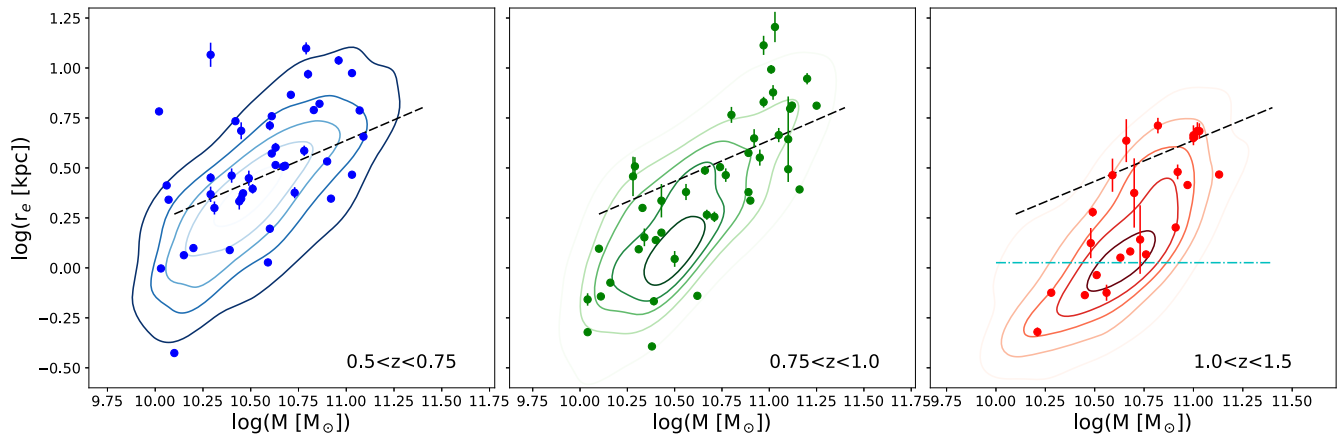


Figure 3. The effective (half-light) radius–stellar mass distribution measured for UVJ-selected galaxies in three redshift bins as indicated in each panel. Here, UVJ-selected, F275W-detected quiescent galaxies are indicated with filled points. Overplotted are density contours (over the range 0%–100%, in 20% decrements) for size–mass distribution of the full UVJ-selected galaxies in the sample. For comparison, the local size–mass relation (black, dashed; S. Shen et al. 2003) is provided in each figure, with F125W FWHM in physical units (at $z \sim 1$) indicated in cyan in the right panel.

$\mu_{F125W} \simeq 29$ mag sq. arcsec $^{-1}$), consistent with the spheroidal/bulge morphology expected for such galaxies.

4.2. Size–Mass Distribution

We provide context for the physical size–stellar mass distribution of the sample quiescent galaxies in Figure 3. Here, for clarity, we include the galaxies well fit²⁰ with GALFIT, separated into three redshift bins (equal in number). Half-light stellar radii and stellar mass measurements for galaxies significantly ($>3\sigma$) detected in F275W at $0.5 \leq z < 0.75$ (blue; left panel), $0.75 \leq z < 1$ (green; center panel), and $1 \leq z \leq 1.5$ (red; right panel) are indicated by filled circles. We overplot size–mass measurements for all UVJ-selected quiescent galaxies in the same color scheme in the panels, with *seaborn* kernel density estimates, as 20% increments between 0% and 100% density.

For ease of comparison, we define a convenience function, “ \bar{x}_r ” to compare the size–mass centroid in a given redshift bin (marginalized over mass) and the local S. Shen et al. (2003) relation (overplotted, black dashed). At $z < 0.75$, the distribution of both the F275-detected and nondetected samples of UVJ-selected galaxies are consistent with the local relationship ($\bar{x}_r \lesssim 1.2$; i.e., sizes are consistent within $\sim 20\%$). At $1 \leq z \leq 1.5$, though, galaxies are uniformly smaller ($\bar{x}_r \sim 2$). Thus, consistent with previous work (L. A. Mowla et al. 2019; K. V. Nedkova et al. 2021), if these galaxies are analogs of progenitors to local quiescent galaxies, the class must undergo moderate size growth.

4.3. Recent Star Formation

Approximately 15% of these UVJ-selected “quiescent” galaxies were significantly detected in F275W (3σ) in UVCANDELS. Recently formed, massive stars are likely the source of this emission; our selection excludes X-ray detected galaxies that may host AGN, and these galaxies are too young cosmologically to have developed evolved stars (e.g., hot horizontal branch or He-enhanced populations; C. Chung et al. 2011; K. Bekki 2012, respectively) most likely responsible for “UV upturn” (S. Yi et al. 1998).

We investigated the observed UV-optical–near-IR SEDs of F275W-detected galaxies with CIGALE (M. Boquien et al. 2019), assuming the galaxy redshift, z_{best} , and optical/near-IR observed photometry from I. G. Momcheva et al. (2016). In this analysis, we fit a library of $\sim 10^7$ models defined by a composite stellar population defined with an “old” (consistent with formation redshift, $z_{\text{form}} \gtrsim 3$) and a “young” (≤ 1 Gyr,²¹ with young-to-total stellar mass fraction, $f_m \in \{10^{-2}, 10^{-1}, 1, 10\}$ [%]) population. These models’ SFHs were defined by either (1) the two-component exponentially declining SFH (CIGALE:sfh2exp) model or (2) a “delayed” exponential burst (CIGALE:sfhdelayed)—in both cases, the ages of the young population were coarsely gridded, $t_{\text{young}}[\text{Myr}] \in \{1, 10, 50, 100, 500, 1000\}$. Stellar populations were developed from G. Bruzual & S. Charlot (2003) models, assuming $Z \in \{Z_{\odot}, 0.5Z_{\odot}\}$ and a S. Charlot & S. M. Fall (2000) dust attenuation model with $A_V \in \{0.0, 0.1, 0.5, 1.0, 1.5, 2.0, 2.5\}$.

Both *sfhdelayed* and *sfh2exp* SFHs were considered in this modeling, as a preference for either in the SED fitting results could constrain the source of RSF as quenched, PSB, and rejuvenated quiescent galaxies have experienced fundamentally different recent SFHs. In recently quenched galaxies, the rapid quenching and subsequent decline into quiescence observed thereafter can be well modeled with truncated SFHs or composite models with multiple, exponentially declining SFHs (K. A. Suess et al. 2022). Alternatively, though dry mergers likely predominate (L. Lin et al. 2010), if “wet” (gas-rich) mergers occur and promote new star formation within an extant quiescent system, this rejuvenated star formation caught “in the act” may be readily discerned as a UV-luminous burst in the SED (K. Rowlands et al. 2017).

In practice, these SFH classes could not be differentiated in this modeling. The reduced χ^2 values measured for the best-fit SED model with either SFH differed by 1% on average for the full sample. Thus, we made no further interpretation of these model fits for differentiating the potential SFHs. We will

²⁰ $1 \lesssim \chi^2_{\nu} \lesssim 5$

²¹ This “young” age limit is set sufficiently high so as to include A-type stellar populations, for which “E+A” galaxies are named (see A. Dressler & J. E. Gunn 1983); the more common sobriquet “poststarburst” encapsulates this class.

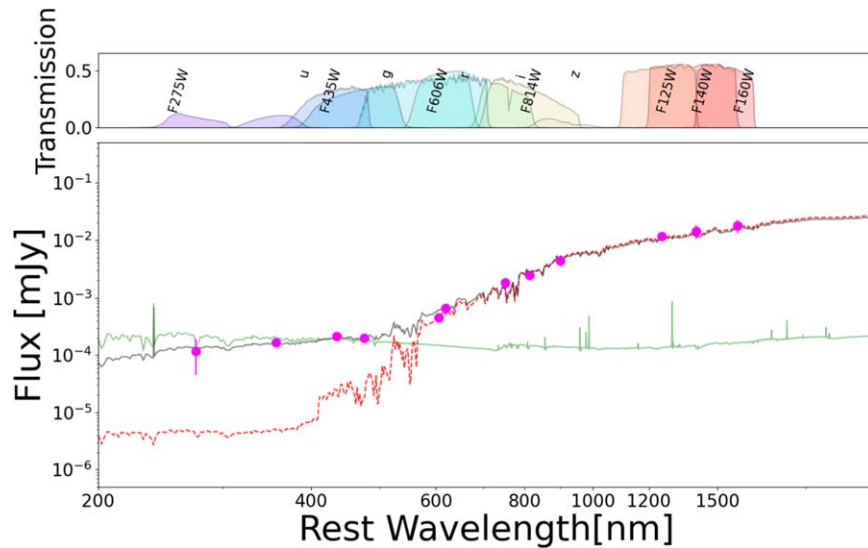


Figure 4. Overplotted on the SED (magenta, filled circles) of this representative UVJ-selected, F275W-detected quiescent galaxy are the best-fit young and old stellar populations (green and red, respectively) with the dust-corrected, best-fit model (black) population. Without UVCANDELS F275W+F435W, the prominent very young ($t_{\text{young}} \simeq 10\text{Myr}$), albeit minor ($f_m \simeq 0.01\%$), stellar population in this “quiescent” galaxy is difficult to characterize. In the top panel, the broadband filtercurves used are provided.

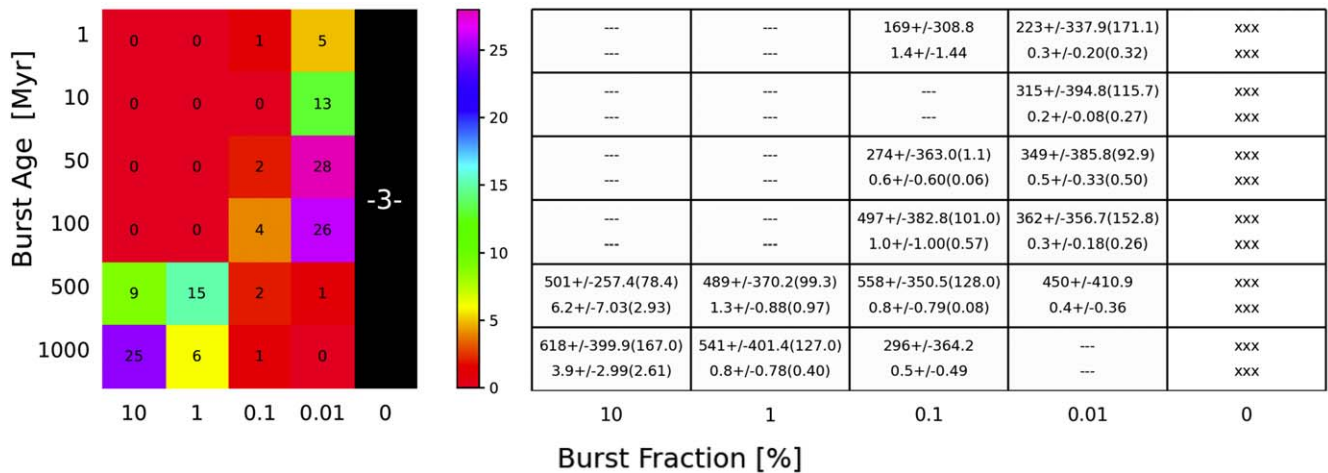


Figure 5. Young stellar age and stellar mass fraction derived with CIGALE (see Section 4 above; M. Boquien et al. 2019) for UVJ-selected, quiescent galaxies with significant F275W ($\geq 3\sigma$) detections. Left panel: a two-dimensional heatmap histogram indicating CIGALE-“best” parameter estimation. Right panel: confidence intervals derived from the CIGALE-“Bayes” parameter estimation for all galaxies in each histogram cell. The upper (lower) row is formatted as follows as “ $x_0 \pm x_1(x_2)$ ”, with x_0 = mean, x_1 = mean error, and x_2 = standard deviation derived for the burst mass (fraction), respectively. Regions of parameter space not populated by galaxies in this sample are indicated by “—”; “xxx” indicates that the CIGALE best-fit SED was inconsistent with young stellar population. When a histogram cell is populated by a single galaxy, $x_2 \equiv 0.00$ is excluded.

discuss extensions to this effort (Section 6) to resolve this degeneracy with new data.

Nonetheless, this analysis provided important, novel constraints on RSF in these galaxies. The UVJ colors of quiescent galaxies typically arise from an old, evolved stellar population in a galaxy with low specific SFR (sSFR), implying a passive evolution for an extended ($\gtrsim 1\text{Gyr}$) timescale. Here, for the quiescent, F275W-detected objects, V. Mehta et al. (2024) in an independent SED analysis report a low average $\log(\text{sSFR}[\text{yr}^{-1}]) \simeq -11.4$. We find a consistent low, average $\log(\text{sSFR}[\text{yr}^{-1}]) \simeq -10.4$ (comparable to the standard threshold on sSFR for quiescent galaxies) while expanding parameter space to include an additional (young) model component. With CIGALE, few ($< 5\%$) of these “quiescent” galaxies have SEDs consistent with *no* RSF, or stellar mass fraction strictly equal to

zero. This result highlights the insensitivity of the UVJ selection criteria for differentiating quiescent galaxies with RSF from the general class of passively evolving massive galaxies (J. Leja et al. 2019). Conversely, we confirm RSF for $> 95\%$ of the F275W-detected galaxies well fit ($\chi^2_\nu < 5$) by these composite (young and old) models using CIGALE.

These UVCANDELS data can improve the age and mass fraction of the young stellar population associated with this RSF, as well. In Figure 4, we plot the observed SED overplotted best-fit model derived with CIGALE of a UV-detected quiescent galaxy, illustrating the utility of these UV data for deriving more robust constraints of the extant stellar populations in such galaxies. For the full sample of UV-detected quiescent galaxies, we summarize in Figure 5 the best-fit model (i.e., lowest χ^2_ν) age and stellar mass fraction of

the young stellar component, with confidence intervals for the best-fit models in each set derived from the CIGALE Bayesian parameter estimations. With a small (2–3) number of independent, broadband rest-frame UV constraints on the SED, this model fitting marginally ($\sim 2\sigma$) identifies RSF as associated with a young population of age, $t \simeq 200$ Myr that is primarily distinguished by the stellar mass fraction.

5. Local Environments

Within hierarchical assembly, mergers are necessarily implicated in the formation and evolution of massive quiescent galaxies (A. F. L. Bluck et al. 2012; T. Carleton et al. 2020; C. J. Conselice et al. 2022; K. A. Suess et al. 2023). A strong correlation of RSF with environment may suggest an enhanced role for such processes. Specifically for this sample, the availability of extensive photometric redshift catalogs (providing a coarse constraint on the density of galaxies in the local environment) makes it possible to meaningfully address the question: “What is the probability that a quiescent galaxy will be identified with RSF, given its local environment?” A question of binary classification such as this, whether a galaxy is detected in F275W or not on the basis of a predictor factor (here, a general measure of environmental richness) is one for which a logistic regression statistical analysis is uniquely well suited and appropriate.

We investigated the potential for environmental effects to promote RSF in these quiescent galaxies. For this measurement, we first defined a uniform volume (spatially: $r \lesssim 120$ kpc; $\theta < 15''$ at $z \approx 1$; in velocity: $\Delta z_{\text{phot}} < 0.1$, or $\sim 2x$ the mean uncertainty on redshift) for all UVJ-selected quiescent galaxies. Using the archival photometric redshift and image data from I. G. Momcheva et al. (2016), $m_{606} \lesssim 25$ objects in this volume were tabulated as “Phot-z Neighbors” to the quiescent galaxy; in velocity space, neighbors were at the redshift of the quiescent galaxy, within 1σ of their measured photometric redshift uncertainty. This measure of “neighbors” is fairly robust to the intrinsic variation by *increased* volume (increasing by $\sim 3\times$) and *decreased* sensitivity (decreasing by $\sim 9\times^{22}$) over the redshift range surveyed. For three equally sized redshift bins, we find a consistent median number of “Phot-z Neighbors” equal to $5 \pm 3.5(1\sigma)$.

Note, this general measure of environment defines a proxy for environmental richness in such a way that these neighbors will likely merger by $z \sim 0$ (see simulations by H.-Y. Jian et al. 2012; T. Tal et al. 2013). We caution against direct comparison between the number of Phot-z Neighbors and other published classifications of group membership, though some may be broadly similar (e.g., “poor groups”; B. M. Poggianti et al. 2009).

We developed a straightforward Markov Chain Monte Carlo (MCMC) model that applies a logistic regression analysis to determine the extent to which the number of neighbors and detection of F275W emission of these quiescent galaxies are correlated. In this analysis, we assumed a sigmoidal distribution, the standard for logistic regression, defined as

$$f(x) = \frac{1}{1 + \exp\{-((\beta_1 \times x) + \beta_0)\}}, \quad (1)$$

²² Surveys with a fixed minimum observed magnitude, such as this one from which we take photometric redshifts, are inclusive of galaxies intrinsically $\sim 9\times$ brighter at the minimum redshift extrema of the full sample.

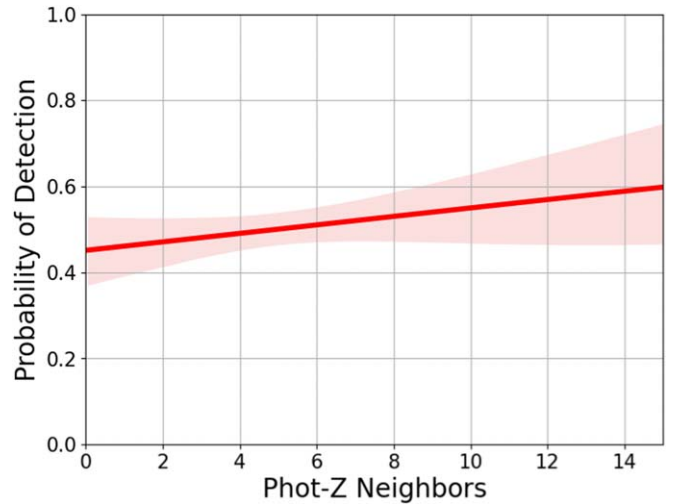


Figure 6. We implemented an MCMC logistic regression statistical analysis to determine the probability of an F275W detection for quiescent galaxies—a signpost for RSF (Section 4.3)—given the number of neighbors. We find the probability of a detection increases marginally with the number of neighbors. This weak environmental correlation likely indicates a reduced role for environmental processes (mergers, interactions), among the array of internal and ex situ processes, in the formation and evolution of quiescent galaxies.

$f(x)$ is the probability of F275W detection and x , the predictor, is the number of Phot-z Neighbors. The terms β_0 and β_1 were defined as normal priors and fitted during the MCMC process: $\beta \sim \text{Norm}(\mu, \sigma)$, where Norm is the univariate normal log likelihood. Specifically, we employed noninformative priors defined by $\beta = \text{Norm}(0, 10)$ such that the probability of detection ultimately measured in this analysis was guided by the predictor itself rather than the choice of prior. We found our model to be relatively robust with varying these priors. Note, RSF is a stochastic, multivariate process of finite duration, and its detection via F275W emission is necessarily dependent on the epoch at which the galaxy is observed. The development and application of a complete, physically motivated suite of priors is beyond the scope of this Letter.

Fundamentally, we used a standard MCMC approach to measure posteriors for each of the β parameters (implemented via `pymc`; J. Salvatier et al. 2016). This MCMC is implemented within a Monte Carlo wrapper though, which ameliorated the disparate sizes of the F275W-detected and nondetected samples. Specifically, in each Monte Carlo (MC) iteration, we defined the predictor array as the concatenation of the F275W-detected sample array and a random draw from the F275W nondetected quiescent galaxies (of the same length as the F275W-detected sample), with the draw weighted to ensure this subsample has a similar distribution of Phot-z Neighbors as the *full* F275W nondetected sample itself. In each MC iteration, we calculated the predictor probabilities (i.e., applying the sigmoid), the F275W detection likelihood was generated (`pymc.Bernouilli`), and with the MCMC we then measured the β parameters. We repeated the MC process 500 times, and recorded the maximum a posteriori (MAP) in each instance. At completion, we averaged the MAP over the full MC run, and confirmed that the MAP does not change significantly (i.e., no flukes occurred in the sampling process). Applying this result, we represent the F275W detection probability in Figure 6, with the 68% maximum credible limits (determined with Python `arviz.hdi`). This analysis yields a *marginal* positive correlation. Quiescent galaxies in richer (larger

numbers of neighbors) environments may be more likely to experience RSF, but the role of the environment in the RSF in quenched or quiescent galaxies appears to be minor.

6. Discussion

Nearly all F275W-detected, UVJ-selected quiescent galaxies are consistent with recent SFH; i.e., $>95\%$ of these galaxies are best-fit with models for which the stellar mass fraction of the young stellar component is *strictly* nonzero. This fraction of all quiescent galaxies surveyed is lower ($\sim 15\%$) than has been historically reported in the literature. Of that fraction, $\sim 60\%$ of quiescent galaxies likely have experienced RSF within the past 100 Myr, but this young population constituted less than $\sim 1\%$ of the total stellar mass, albeit with considerable uncertainty. We note that only a small subset ($\sim 1\%$) of these F275W-detected quiescent galaxies with confirmed RSF from SED modeling are identified with weak ($\sim 3\text{--}5\sigma$) H α emission. Thus, these HST UV data were critical for identifying and characterizing RSF in large area imaging surveys of quiescent galaxy evolution.

Mergers and interactions in particular have been targeted for studies to characterize the frequency and dominance over cosmic time of the internal and ex situ process driving quiescent galaxy evolution. In these efforts, morphological evidence of merger activity in, e.g., rejuvenating quiescent galaxies is rare in the local Universe (R. M. Crockett et al. 2012); at low redshift morphological proxies for mergers (C. J. Conselice 2003) or correlations with, e.g., environmental density (see, e.g., C. Cleland & S. L. McGee 2021; S. Wilkinson et al. 2022) are used to infer the role for mergers. In hierarchical assembly, galaxy merger rates are expected to correlate with environment and increase with decreasing mass ratio of the mergers, as demonstrated in cosmological simulations (O. Fakhouri & C.-P. Ma 2009; H.-Y. Jian et al. 2012). Note, recent observations at $z \lesssim 0.3$ indicate, among field or group massive quiescent galaxies, the ensemble major merger fraction may in fact be weakly or *anticorrelated* with environmental richness (W. J. Pearson et al. 2024; U. Sureshkumar et al. 2024).

We found a *marginal* positive correlation between the number of neighbors and RSF. If molecular gas accretion to massive, quiescent galaxies through mergers and interactions promoted the observed RSF (D. R. Patton et al. 2020), this weak correlation could suggest a minor role specifically for *gas-rich* (wet) accretion, supporting independent conclusions inferred from optical morphology (Z. Ji & M. Giavalisco 2022). Alternatively, RSF may arise in recently quenched galaxies manifesting as PSBs. Such galaxies constitute increasingly large fractions of galaxies in increasingly dense environments (B. M. Poggianti et al. 2009; A. Paccagnella et al. 2019), but the marginal correlation suggests a minor role for mergers and by implication, a more pronounced role for other (e.g., AGN; X-ray *faint* given our selection) feedback modes (R. J. Smethurst et al. 2016; I. Martin-Navarro et al. 2022). Note, few of the sample galaxies are spatially resolved in the UVCANDELS F275W images, but in future work we will investigate UV-optical color gradients, extending recent efforts at longer wavelengths (Y. Guo et al. 2011; Z. Ji & M. Giavalisco 2023; C. M. Cheng et al. 2024) to characterize the assembly histories of the galaxies. This analysis could assist in revealing the extent to which mergers and interactions enhance the predominant smooth accretion mode identified by simulations (see H. Padmanabhan & A. Loeb 2020).

Finally, high-resolution rest-frame optical–near-IR spectra are important for advancing the effort presented in this Letter. First, spectroscopic redshifts improve the assessment of the environment (close pair and group identification and velocity dispersions therein) over what can be achieved with the photometric and grism redshifts primarily relied upon in this work. Furthermore, improved stellar mass and companion SFHs allow for the extensions of the logistic regression analysis in Section 5 to additional predictors (e.g., quiescent to companion stellar mass ratios, useful for discriminating major and minor mergers). Second, high-resolution spectra are critical for identifying the specific RSF modality: rejuvenation or PSB. For example, PSBs are often identified amongst quiescent galaxies on the basis of strong Balmer absorption²³ that is difficult to observe via low-resolution HST grism spectroscopy for individual galaxies. Further, the truncated SFH of these galaxies is not readily distinguished by UV-optical-near IR broadband data alone (see K. A. Suess et al. 2022). Distinguishing PSBs from rejuvenated galaxies in this sample constrains the pathway to quiescence, which has broader applicability for questions of quiescent galaxy evolution. For example, Y. Zhang et al. (2024) recently selected PSBs from the Dark Energy Survey and measured near-IR stellar sizes using HST. They found that PSBs were typically smaller than the extant quiescent galaxy population. The authors suggest that (dry, minor) mergers could drive the size–mass growth of these galaxies. Determining the primary pathway by which progenitors of modern quiescent galaxies evolve from high-redshift galaxies is made difficult by the selection of PSBs alone, which—as the authors state—may be a biased progenitor set. In this Letter, we show the utility of high spatial resolution imaging and rest-frame UV sensitivity for differentiating quiescent galaxies with and without RSF. When these data are combined with high-resolution spectroscopic data necessary for precise SFHs and more robust classification of the local environment, the mode(s) by which galaxies transform from star forming to quiescent over cosmic time will be more readily constrained.

7. Conclusions

We have combined UVCANDELS F275W+F435W imaging with archival rest-frame optical–near-IR photometry to investigate the class of UVJ color–color selected quiescent galaxies at $0.5 < z < 1.5$. Applying this long baseline of wavelength coverage observed with HST over a decade, we determined $\sim 15\%$ to have experienced RSF ($t < 1$ Gyr ago, with mass fraction $-1 < \log(f_{M\star}) < -3$). We performed a logistic regression statistical analysis to test for a correlation of RSF with environmental richness. We found the RSF to be only marginally positively correlated with the environmental richness. This correlation—combined with the relatively small total mass in young stars—may imply a weak role for the environmental processes in the evolution of this class of recently star-forming massive quiescent galaxies. Future efforts to further differentiate the modes of RSF will benefit from a high-resolution spectroscopic campaign of the quiescent galaxies and their near-field companions.

²³ Though not standardized, PSBs are often selected on H δ absorption strength (H $\delta > 5$; e.g., T. Goto et al. 2003; K. Alatalo et al. 2016), with other constraints commonly employed (e.g., (NUV- g') color, H. M. Yesuf et al. 2017)










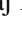








Acknowledgments

This research is partly based on observations made with the NASA/ESA Hubble Space Telescope obtained from the Space Telescope Science Institute, which is operated by the Association of Universities for Research in Astronomy, Inc., under NASA contract NAS 5-26555. These observations are associated with program(s) HST-GO-15647. This research used archival data and value-added catalogs hosted by the Mikulski Archive for Space Telescopes at the Space Telescope Science Institute from the HST-GO-11600, HST-GO-12060, HST-GO-12099, HST-GO-12177, and HST-GO-12328 programs. We thank an anonymous referee whose insightful comments were helpful in the presentation of the data and analysis. M.R. acknowledges his late father, Melvin, for helpful discussions. X.W. is supported by the National Natural Science Foundation of China (grant 12373009), the CAS Project for Young Scientists in Basic Research grant No. YSBR-062, the Fundamental Research Funds for the Central Universities, the Xiaomi Young Talents Program, and the science research grant from the China Manned Space Project. X.W. also acknowledges work carried out, in part, at the Swinburne University of Technology, sponsored by the ACAMAR visiting fellowship.

Facilities: HST (WFC3), MAST (HLSP).

Software: ASTROPY (Astropy Collaboration et al. 2013; 2022), GALFIT (C. Y. Peng et al. 2002; Y.-j. Peng et al. 2010), CIGALE (M. Boquien et al. 2019), MATPLOTLIB (J. D. Hunter 2007), SEABORN (M. L. Waskom 2021).

ORCID iDs

Michael J. Rutkowski  <https://orcid.org/0000-0001-7016-5220>
 Bonnabelle Zabelle  <https://orcid.org/0000-0002-7830-363X>
 Tyler Hagen  <https://orcid.org/0009-0007-2936-1124>
 Anahita Alavi  <https://orcid.org/0000-0002-8630-6435>
 Seth Cohen  <https://orcid.org/0000-0003-3329-1337>
 Christopher Conselice  <https://orcid.org/0000-0003-1949-7638>
 Norman Grogin  <https://orcid.org/0000-0001-9440-8872>
 Yicheng Guo  <https://orcid.org/0000-0003-2775-2002>
 Matthew Hayes  <https://orcid.org/0000-0001-8587-218X>
 Sugata Kaviraj  <https://orcid.org/0000-0002-5601-575X>
 Anton Koekemoer  <https://orcid.org/0000-0002-6610-2048>
 Ray A. Lucas  <https://orcid.org/0000-0003-1581-7825>
 Kameswara Bharadwaj Mantha  <https://orcid.org/0000-0002-6016-300X>
 Alec Martin  <https://orcid.org/0000-0002-6632-4046>
 Vihang Mehta  <https://orcid.org/0000-0001-7166-6035>
 Bahram Mobasher  <https://orcid.org/0000-0001-5846-4404>
 Nimish Hathi  <https://orcid.org/0000-0001-6145-5090>
 Kalina V. Nedkova  <https://orcid.org/0000-0001-5294-8002>
 Robert O'Connell  <https://orcid.org/0000-0002-8190-7573>
 Marc Rafelski  <https://orcid.org/0000-0002-9946-4731>
 Claudia Scarlata  <https://orcid.org/0000-0002-9136-8876>
 Harry I. Teplitz  <https://orcid.org/0000-0002-7064-5424>
 Xin Wang  <https://orcid.org/0000-0002-9373-3865>
 Rogier Windhorst  <https://orcid.org/0000-0001-8156-6281>
 L. Y. Aaron Yung  <https://orcid.org/0000-0003-3466-035X>

References

Alatalo, K., Lisenfeld, U., Lanz, L., et al. 2016, *ApJ*, 827, 106
 Alavi, A., Siana, B., Richard, J., et al. 2014, *ApJ*, 780, 143
 Anderson, J., Baggett, S., & Kuhn, B. 2021, Instrument Science Report 2021-9, Baltimore, MD: Space Telescope Science Institute

Astropy Collaboration, Price-Whelan, A. M., Lim, P. L., et al. 2022, *ApJ*, 935, 167
 Astropy Collaboration, Robitaille, T. P., Tollerud, E. J., et al. 2013, *A&A*, 558, A33
 Bekki, K. 2012, *ApJ*, 747, 78
 Bekki, K., Couch, W. J., Shioya, Y., & Vazdekis, A. 2005, *MNRAS*, 359, 949
 Belfiore, F., Maiolino, R., Bundy, K., et al. 2018, *MNRAS*, 477, 3014
 Biretta, J., Van Orsow, D., Sparks, W., Reinhart, M., & Vick, A. 2003, Instrument Science Report ACS 2003-05, Baltimore, MD: Space Telescope Science Institute
 Bluck, A. F. L., Conselice, C. J., Buitrago, F., et al. 2012, *ApJ*, 747, 34
 Boquien, M., Burgarella, D., Roehly, Y., et al. 2019, *A&A*, 622, A103
 Bower, G. G., Lucey, J. R., & Ellis, R. S. 1992, *MNRAS*, 254, 589
 Bruzual, G., & Charlot, S. 2003, *MNRAS*, 344, 1000
 Carleton, T., Guo, Y., Nayyeri, H., et al. 2020, *MNRAS*, 491, 2822
 Carnall, A. C., McLure, R. J., Dunlop, J. S., et al. 2023a, *Natur*, 619, 716
 Carnall, A. C., McLeod, D. J., McLure, R. J., et al. 2023b, *MNRAS*, 520, 3974
 Cassata, P., Giavalisco, M., Guo, Y., et al. 2011, *ApJ*, 743, 96
 Charlot, S., & Fall, S. M. 2000, *ApJ*, 539, 718
 Cheng, C. M., Kriek, M., Beverage, A. G., et al. 2024, *MNRAS*, 532, 3604
 Chung, C., Yoon, S.-J., & Lee, Y.-W. 2011, *ApJL*, 740, L45
 Clausen, M., Whitaker, K. E., Momcheva, I., et al. 2024, *ApJ*, 971, 99
 Cleland, C., & McGee, S. L. 2021, *MNRAS*, 500, 590
 Conselice, C. J. 2003, *ApJS*, 147, 1
 Conselice, C. J., Mundy, C. J., Ferreira, L., & Duncan, K. 2022, *ApJ*, 940, 168
 Crockett, R. M., Shabala, S. S., Kaviraj, S., et al. 2012, *MNRAS*, 421, 1603
 Cutler, S. E. 2024, arXiv:2312.1501
 de Graaff, A., Setton, D. J., Brammer, G., et al. 2025, *NatAs*, 9, 280
 Dome, T., Tacchella, S., Fialkov, A., et al. 2024, *MNRAS*, 527, 2139
 Dressler, A., & Gunn, J. E. 1983, *ApJ*, 270, 7
 Dubois, Y., Gavazzi, R., Peirani, S., & Silk, J. 2013, *MNRAS*, 433, 3297
 El-Badry, K., Wetzel, A., Geha, M., et al. 2016, *ApJ*, 820, 131
 Fakhouri, O., & Ma, C.-P. 2009, *MNRAS*, 394, 1825
 Gelli, V., Pallottini, A., Salvadori, S., et al. 2025, arXiv:2501.16418
 Glazebrook, K., Schreiber, C., Labbé, I., et al. 2017, *Natur*, 544, 71
 Goto, T., Nichol, R. C., Okamura, S., et al. 2003, *PASJ*, 55, 771
 Grogin, N. A., Kocevski, D. D., Faber, S. M., et al. 2011, *ApJS*, 197, 35
 Guo, Y., Giavalisco, M., Cassata, P., et al. 2011, *ApJ*, 735, 18
 Heavens, A., Panter, B., Jimenez, R., & Dunlop, J. 2004, *Natur*, 428, 625
 Hunter, J. D. 2007, *CSE*, 9, 90
 Ilbert, O., McCracken, H. J., Le Fèvre, O., et al. 2013, *A&A*, 556, A55
 Ji, Z., & Giavalisco, M. 2022, *ApJ*, 935, 120
 Ji, Z., & Giavalisco, M. 2023, *ApJ*, 943, 54
 Jian, H.-Y., Lin, L., & Chiueh, T. 2012, *ApJ*, 754, 26
 Johansson, J., Thomas, D., & Maraston, C. 2012, *MNRAS*, 421, 1908
 Kaviraj, S., Devriendt, J., Dubois, Y., et al. 2015, *MNRAS*, 452, 2845
 Kaviraj, S., Khochfar, S., Schawinski, K., et al. 2008, *MNRAS*, 388, 67
 Kaviraj, S., Rowlands, K., Alpaslan, M., et al. 2013, *MNRAS*, 435, 1463
 Kaviraj, S., Schawinski, K., Devriendt, J. E. G., et al. 2007, *ApJS*, 173, 619
 Kim, K., Malhotra, S., Rhoads, J. E., et al. 2018, *ApJ*, 867, 118
 Koekemoer, A. M., Faber, S. M., Ferguson, H. C., et al. 2011, *ApJS*, 197, 36
 Leja, J., Tacchella, S., & Conroy, C. 2019, *ApJL*, 880, L9
 Lin, L., Cooper, M. C., Jian, H.-Y., et al. 2010, *ApJ*, 718, 1158
 Looser, T. J., D'Eugenio, F., Maiolino, R., et al. 2024, *Natur*, 629, 53
 Martín-Navarro, I., Shankar, F., & Mezcuza, M. 2022, *MNRAS*, 513, L10
 Mehta, V., Teplitz, H. I., Scarlata, C., et al. 2023, *ApJ*, 952, 133
 Mehta, V., Rafelski, M., Sunnquist, B., et al. 2024, *ApJS*, 275, 17
 Momcheva, I. G., Brammer, G. B., van Dokkum, P. G., et al. 2016, *ApJS*, 225, 27
 Mowla, L. A., van Dokkum, P., Brammer, G. B., et al. 2019, *ApJ*, 880, 57
 Muzzini, A., Marchesini, D., Stefanon, M., et al. 2013, *ApJ*, 777, 18
 Naab, T., Johansson, P. H., & Ostriker, J. P. 2009, *ApJL*, 699, L178
 Nedkova, K. V., Häußler, B., Marchesini, D., et al. 2021, *MNRAS*, 506, 928
 Nedkova, K. V., Rafelski, M., Teplitz, H. I., et al. 2024, *ApJ*, 970, 188
 Oke, J. B., & Gunn, J. E. 1983, *ApJ*, 266, 713
 Paccagnella, A., Vulcani, B., Poggianti, B. M., et al. 2019, *MNRAS*, 482, 881
 Padmanabhan, H., & Loeb, A. 2020, *MNRAS*, 496, 1124
 Paspaliaris, E. D., Xilouris, E. M., Nersesian, A., et al. 2023, *A&A*, 669, A11
 Patton, D. R., Wilson, K. D., Metrow, C. J., et al. 2020, *MNRAS*, 494, 4969
 Pearson, W. J., Santos, D. J. D., Goto, T., et al. 2024, *A&A*, 686, A94
 Peng, C. Y., Ho, L. C., Impey, C. D., & Rix, H.-W. 2002, *AJ*, 124, 266
 Peng, Y.-j., Lilly, S. J., Kovač, K., et al. 2010, *ApJ*, 721, 193
 Planck Collaboration, Ade, P. A. R., Aghanim, N., et al. 2016, *A&A*, 594, A13
 Poggianti, B. M., Aragón-Salamanca, A., Zaritsky, D., et al. 2009, *ApJ*, 693, 112
 Prichard, L. J., Rafelski, M., Cooke, J., et al. 2022, *ApJ*, 924, 14

- Rafelski, M., Teplitz, H. I., Gardner, J. P., et al. 2015, *AJ*, 150, 31
- Rowlands, K., Wild, V., Bourne, N., et al. 2017, *MNRAS*, 473, 1168
- Rutkowski, M. J., Jeong, H., Cohen, S. H., et al. 2014, *ApJ*, 796, 101
- Ryan, R. E. J., McCarthy, P. J., Cohen, S. H., et al. 2012, *ApJ*, 749, 53
- Salim, S., Boquien, M., & Lee, J. C. 2018, *ApJ*, 859, 11
- Salvatier, J., Wiecki, T. V., & Fonnesbeck, C., 2016 PyMC3: Python Probabilistic Programming Framework, Astrophysics Source Code Library, ascl:1610.016
- Shen, S., Mo, H. J., White, S. D. M., et al. 2003, *MNRAS*, 343, 978
- Smethurst, R. J., Lintott, C. J., Simmons, B. D., et al. 2016, *MNRAS*, 463, 2986
- Smith, B. M., Windhorst, R. A., Teplitz, H., et al. 2024, *ApJ*, 964, 73
- Strait, V., Brammer, G., Muzzin, A., et al. 2023, *ApJL*, 949, L23
- Suess, K. A., Leja, J., Johnson, B. D., et al. 2022, *ApJ*, 935, 146
- Suess, K. A., Williams, C. C., Robertson, B., et al. 2023, *ApJ*, 956, L42
- Sureshkumar, U., Durkalec, A., Pollo, A., et al. 2024, *A&A*, 686, A40
- Tal, T., van Dokkum, P. G., Franx, M., et al. 2013, *ApJ*, 769, 31
- Teplitz, H., Wang, X., Prichard, L., et al. 2022, Ultraviolet Imaging of the Cosmic Assembly Near-infrared Deep Extragalactic Legacy Survey Fields (UVCANDELS), STScI/MAST, doi: 10.17909/8S31-F778
- Valentino, F., Tanaka, M., Davidzon, I., et al. 2020, *ApJ*, 889, 93
- van der Wel, A., Bell, E. F., Häussler, B., et al. 2012, *ApJS*, 203, 24
- Verrico, M. E., Setton, D. J., Bezanson, R., et al. 2023, *ApJ*, 949, 5
- Wang, X., Teplitz, H. I., Smith, B. M., et al. 2025, *ApJ*, 980, 74
- Waskom, M. L. 2021, *JOSS*, 6, 3021
- Wild, V., Almaini, O., Dunlop, J., et al. 2016, *MNRAS*, 463, 832
- Wilkinson, S., Ellison, S. L., Bottrell, C., et al. 2022, *MNRAS*, 516, 4354
- Williams, R. J., Quadri, R. F., Franx, M., van Dokkum, P., & Labbé, I. 2009, *ApJ*, 691, 1879
- Yesuf, H. M., French, K. D., Faber, S. M., & Koo, D. C. 2017, *MNRAS*, 469, 3015
- Yi, S., Demarque, P., & Oemler, A. J. 1998, *ApJ*, 492, 480
- Zabelle, B., Scarlata, C., Mehta, V., et al. 2023, *ApJ*, 947, 17
- Zhang, Y., Setton, D. J., Price, S. H., et al. 2024, *ApJ*, 976, 36